Long Tubular Penetration Models

Minhyung Lee and Stephan Bless
Institute for Advanced Technology
The University of Texas at Austin

March 1996

IAT.R 0096

Institute for Advanced Technology
The University of Texas at Austin

19961209 025

REPORT DOCUMENTATION PAGE

Form Approved
OMB NO. 0704-0188

1. AGENCY USE ONLY (Leave blank)	2. REPORT DATE March 1996	3. REPORT TYPE AND DATES COVERED Technical Report , DEC 1995 -- JAN 1996

4. TITLE AND SUBTITLE

Long Tubular Penetration Models

5. FUNDING NUMBERS

Contract # DAAA21-93-C-0101

6. AUTHOR(S)

M. Lee and S. Bless

7. PERFORMING ORGANIZATION NAME(S) AND ADDRESS(ES)

Institute for Advanced Technology
The University of Texas at Austin
4030-2 W. Braker Lane, #200
Austin, TX 78759

8. PERFORMING ORGANIZATION REPORT NUMBER

IAT.R 0096

9. SPONSORING / MONITORING AGENCY NAME(S) AND ADDRESS(ES)

U.S. Army Research Laboratory
ATTN: AMSRL-WT-T
Aberdeen Proving Ground, MD 21005-5066

10. SPONSORING / MONITORING AGENCY REPORT NUMBER

11. SUPPLEMENTARY NOTES

The view, opinions and/or findings contained in this report are those of the author(s) and should not be considered as an official Department of the Army position, policy, or decision, unless so designated by other documentation.

12a. DISTRIBUTION / AVAILABILITY STATEMENT

Approved for public release; distribution unlimited.

12b. DISTRIBUTION CODE

A

13. ABSTRACT *(Maximum 200 words)*

The penetration mechanics of a thick walled tubular penetrator is examined as ratio of the outer to inner diameter is increased from values of 0.4 to 0.74. Since the craters are characterized by depth and radius, analytical models for the crater radius due to tubular penetrators are developed. A two stage cavity expansion model is provided, which is based on the observations that in the first stage, the eroded penetration element exerts pressure on the target and opens a cavity. In the second stage, the inertia imparted to the target is responsible for the further expansion of the cavity. The analysis includes the centrifugal force exerted by the penetrator, radial inertia of the target, and the strength of the target. The crater radius is also determined from the energy and momentum principles and the results are compared with other results. The results obtained from the momentum principle provide good agreement with the other models in spite of its simplicity. The penetration velocity for tubes, which is less than that of rods, thus cannot be obtained from the modified hydrodynamic theory, is determined from computer simulations on behalf of the penetration efficiency. Numerical simulations using AUTODYN-2D are conducted for comparison with the analytical predictions and these confirm the phenomenological assumptions in the models.

14. SUBJECT TERMS

tubular penetrator, crater radius, target inertia, two stage cavity expansion model, centrifugal force, mushrooming effect

15. NUMBER OF PAGES

16

16. PRICE CODE

17. SECURITY CLASSIFICATION OF REPORT Unclassified	18. SECURITY CLASSIFICATION OF THIS PAGE Unclassified	19. SECURITY CLASSIFICATION OF ABSTRACT Unclassified	20. LIMITATION OF ABSTRACT UL

Contents

List of Figures

List of Tables

Long Tubular Penetration Models

Minhyung Lee and Stephan Bless

ABSTRACT

The penetration mechanics of a thick walled tubular penetrator is examined as ratio of the outer to inner diameter is increased from values of 0.4 to 0.74. Since the craters are characterized by depth and radius, analytical models for the crater radius due to tubular penetrators are developed. A two stage cavity expansion model is provided, which is based on the observations that in the first stage, the eroded penetration element exerts pressure on the target and opens a cavity. In the second stage, the inertia imparted to the target is responsible for the further expansion of the cavity. The analysis includes the centrifugal force exerted by the penetrator, radial inertia of the target, and the strength of the target.

The crater radius is also determined from the energy and momentum principles and the results are compared with other results. The results obtained from the momentum principle provide good agreement with the other models in spite of its simplicity. The penetration velocity for tubes, which is less than that of rods, thus cannot be obtained from the modified hydrodynamic theory, is determined from computer simulations on behalf of the penetration efficiency.

Numerical simulations using AUTODYN-2D are conducted for comparison with the analytical predictions and these confirm the phenomenological assumptions in the models.

I. INTRODUCTION

Although the penetration mechanics of long rods is well understood, this is not the case for tubular penetrators. The radial motion of target material due to rod hypervelocity penetrations occurs in two stages as shown in numerical simulations [1]. In the first stage, eroded penetrator elements play the dominant roles in opening a cavity. In the second stage, the inertia deposited in the target is responsible for further cavity growth until the strength of the target forces it to come to rest.

An earlier analysis of hypervelocity penetration of slender hollow cylinders into homogeneous targets is given in Franzen [2]; it is based on hydrodynamic theory. Even though many simplifications are made, the model can provide a criteria for the choking of flow on the tube axis. This condition occurs for the ratio of the inner diameter to outer diameter, μ, less than 0.7.

1

In the present work, for $\mu < 0.7$ simple analytical models for describing cavity growth and resulting final crater size in the target are developed in three ways. These models were already applied for the penetration of rods [3]. The first analytical model is based on the method of Franzen [2] for the purpose of determining the extent of the first stage cavity expansion due to eroded penetrator elements. Because of the neglect of the target strength in Franzen's model, the cavity radius is not bounded. Including the target strength term in the analysis allows us to explore the ultimate cavity radius achieved during the first stage cavity expansion, which is solely due to radial movement in the penetrator "mushrooming". To estimate the amount of inertia imparted to the target in the second stage cavity expansion model, for simplicity, we use an energy principle. The energy and momentum principles are also developed to determine the final crater size and the results are compared with other results.

An axisymmetric coordinate system moving at the constant penetration velocity U is used as reference. All lengths are scaled by the outer radius r_p of the tubular penetrator, thus dimensions are characterized by the inner radius $\mu < 1$. The outer radius varies with μ. Numerical simulations using AUTODYN-2D are also presented for comparison with the analytical predictions.

II. ENERGY BALANCE

The crater size for penetration of long tubular penetrators is described in this section within the framework of energy balance. The basic assumptions required in the analyses are:

- Target material is considered as incompressible and inviscid flow.
- The motion of the cavity wall is purely radial.
- The internal energy change due to thermal effects and strain energy in the target are negligible.
- Work done against the projectile during penetration is negligible.
- Steady state is assumed.

- **The kinetic energy loss of a penetrator per unit target length.**

Consider a long tubular penetrator of density ρ_p, inner radius μ and length L impacting at normal incidence an infinite target of density ρ_t. For steady state penetration the loss of kinetic energy of a penetrator per unit target length equals the total energy deposited in the unit target length. The loss of kinetic energy of the tubular penetrator per unit target length is given by,

$$E_{kP} = \frac{1}{2}\left(\frac{m}{P}\right)V^2 ,$$

(1)

where $m = \rho_p \pi (1 - \mu^2) L$. Here m is the mass, L is the penetrator length, P is the penetration depth, and V is the impact velocity. Using the hydrodynamic relation $L/P = (V - U)/U$, Eq. (1) becomes,

$$E_{kP} = \frac{1}{2} \rho_p \pi (1 - \mu^2) \frac{(V - U)}{U} V^2 . \tag{2}$$

The amount of plastic work per unit target length done to open the outside cavity is given by,

$$E_{pt} = \int_{\mu}^{a_c} (2\pi r) R_t \, dr = \pi (a_c^2 - \mu^2) R_t , \tag{3}$$

where R_t is the target resistance for radial cavity expansion. If it is further assumed that target material within μ flows up the axis of the penetration and is in a uniaxial compressive state, the work done for the inner target material per unit length, E_{pti}, is given by,

$$E_{pti} = \pi \mu^2 Y_p . \tag{4}$$

The velocity field vanishes throughout the flow field after a maximum cavity is formed, yielding zero kinetic energy in the target. Details may be found in Ref. [3]. At this time the conservation of the energy can be expressed by the relation,

$$E_{kp} = \pi (a_c^2 - \mu^2) R_t + \pi \mu^2 Y_p . \tag{5}$$

Combining Eqs. (3), (4) and (5) leads to a final crater size of,

$$\frac{a_c}{r_p} = \sqrt{\frac{1/2 \rho_p (1 - \mu^2) V^2}{R_t} \frac{(V - U)}{U} + \frac{\mu^2 (R_t - Y_p)}{R_t}} . \tag{6}$$

This expression applies to rods if μ equals zero.

— **Determination of the penetration velocity.**

An important parameter to be determined in the tubular case is the penetration velocity which cannot be predicted from the "modified" Bernoulli equation. For steady state penetration the modified Bernoulli equation applies,

$$1/2 \rho_p (V - U)^2 + Y_p = 1/2 \rho_t U^2 + R_t . \tag{7}$$

Then U is given by [4],

$$U = \frac{V - \alpha\sqrt{V^2 + 2(1 - \alpha^2)(R_t - Y_p)/\rho_t}}{(1 - \alpha^2)} , \qquad (8)$$

where $\alpha = \sqrt{\rho_t / \rho_p}$. For thick tubes, most of the penetrator material flows to the outside of the cavity, and yields a larger crater diameter. In this case, the penetration velocity will be smaller than predicted by Eq. (8), thus resulting in poor penetration efficiency. If it is further assumed for steady state penetration that the tubular penetration efficiency $(P/L)_{tube}$ is related to the rod penetration efficiency $(P/L)_{rod}$ by,

$$\frac{(P/L)_{tube}}{(P/L)_{rod}} = \frac{\left(U/(V-U)\right)_{tube}}{\left(U/(V-U)\right)_{rod}} = \lambda , \qquad (9)$$

where λ is a constant to be determined from computer simulations. The penetration velocity of tubular penetrator U_{tube} is then given by,

$$U_{tube} = \frac{\lambda V U_{rod}}{V - (1 - \lambda) U_{rod}} . \qquad (10)$$

where U_{rod} is the penetration velocity of a rod penetrator. The theoretical R_t values determined by the classical spherical cavity expansion model as presented by Satapathy and Bless [5] is used in the present work:

$$R_t = -\frac{2}{3} Y \, ln\left(\frac{Y}{2G}\right) + \frac{2}{3} Y , \qquad (11)$$

which gives RHA steel the value $R_t = 5.0$ GPa.

III. MOMENTUM PRINCIPLES

The crater size for penetration of long tubular penetrators is described in this section within the framework of momentum arguments. The control volume attached to the penetration interface of two bodies is shown in Fig. 1. The control volume is bounded on the left by the penetration interface, on the right by the Hugoniot elastic-plastic interface, and on the top and bottom by the material interfaces. The penetration interface is moving with velocity U. Mass enters the control volume through the elastic-plastic interface.
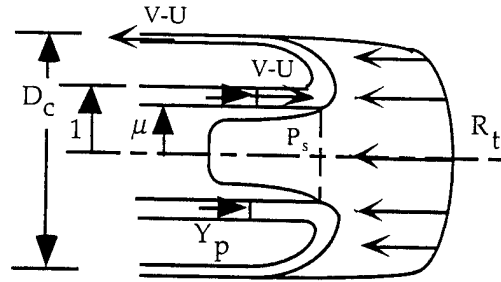
4

Fig. 1. Control volume.

For thick tubes, only target material moves through the inner cavity. This flow can be considered incompressible and the Bernoulli's theorem is applicable [2]. If U is smaller than the sound speed in the target, the static pressure at the inner cavity entrance $P_s(\mu)$ becomes smaller than the stagnation pressure $1/2\rho_t U^2$. To determine this static pressure, it is necessary to obtain the local inner cavity radius. After a short transient phase this static pressure is created near the center of the axisymmetric axis such that it pushes most of the projectile material to the outside cavity. The static pressure will decrease from its initial value to zero at the throat. From the Bernoulli's theorem with a mass conservation in the flow through the cavity, the static pressure at the inner cavity entrance is given by [2],

$$P_s(\mu) = \frac{1}{2}\rho_t U^2 \left[1 - \left(\frac{\mu_t}{\mu}\right)^4 \right],$$ (12)

where μ_t is the cavity radius at the throat, which is not determined for thick tubes [2]. Now the static pressure at the entrance is assumed to be the stagnation pressure. For example at $\mu_t/\mu = 0.5$, the relative error is 0.0625.

To approximately determine the final crater size, the conservation of momentum equation for the control volume is,

$$R_t(\frac{\pi}{4}D_c^2) - 4Y_p\frac{\pi}{4}(1-\mu^2) - 4\frac{1}{2}\rho_t U^2 \frac{\pi}{4}(\mu^2) = 2\rho_p 4\frac{\pi}{4}(1-\mu^2)(V-U)^2,$$ (13)

where D_c is the normalized crater diameter. The conservation of mass for the control volume is accounted for in this equation by equating the incoming mass to the outgoing mass in a steady state condition. The solution to the final crater radius is then given by,

$$\frac{a_c}{r_p} = \sqrt{\frac{(1-\mu^2)Y_p}{R_t} + \frac{1/2\rho_t U^2\mu^2}{R_t} + \frac{2\rho_p(1-\mu^2)(V-U)^2}{R_t}}.$$ (14)

If μ equals zero, this expression gives the same result previously obtained for rod penetrations [3].

IV. TWO STAGE CAVITY EXPANSION MODEL (TSCEM)

We propose that in the first stage, the eroded penetrator elements exert pressure on the target and open a cavity. In the second stage, the inertia imparted to the target is responsible for the further expansion of the cavity, especially at hypervelocity penetration rates. It is further hypothesized that the final cavity radius is equal to the sum of the cavity radii produced by each stage acting independently, regardless of the order of application of loads. In other words, we use the principle of superposition for the total work done by each stage. The analysis includes the centrifugal force exerted by the penetrator, radial inertia of the target, and the strength of the target. The basic assumptions required in the analysis are:

— Target material flow is considered as incompressible, steady and inviscid relative to the stagnation region.

— The pressure profile exerted by the target is assumed to be $1/2\rho_t U^2 \sin^3\beta$ as provided in Ref. [6], where β is the angle between the tangent direction of the centerline and the axis of symmetry. The variation in velocity of the "mushrooming" penetrator material is normal to the "mushrooming" surface tangent. Although the Newtonian pressure, $1/2\rho_t U^2 \sin^2\beta$, allows a simple closed-form solution it over-predicts the pressure profile [6]. This pressure is acting normal to the flow at radius r, where r is the radius of the centerline of an eroded penetrator element.

— The stagnation region over which the pressure equals $1/2\rho_t U^2$ exists for $\pi \leq \beta \leq \pi/2$. The domain for the outside of the stagnation region is $0 \leq \beta \leq \pi/2$.

— For the inertia calculation, we make an analogy with the case of a rigid body penetrator as we did in Ref. [3]. The physical assumption is that a penetrator head moving at constant velocity U transfers kinetic energy to the target. For simplicity, the energy method described in the previous model is then adopted.

1. The First Stage Cavity Expansion

With these assumptions, the first stage cavity expansion can be derived from Franzen's analysis [2] with presence of the strength of the target. The target strength will eventually halt the cavity growth. The geometry of the two stage cavity expansion model (TSCEM) is shown in Fig. 2.
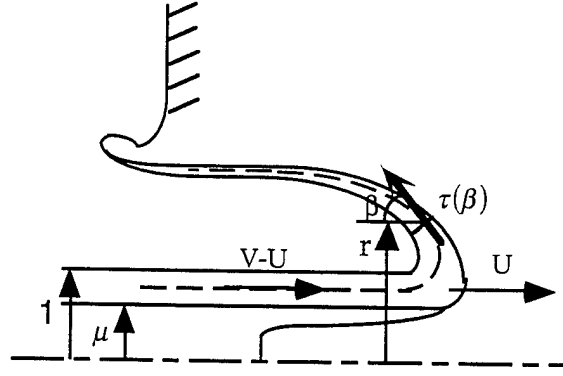
Fig. 2. Geometry of the two stage cavity expansion model.

From mass conservation in a coordinate system located at the penetration front and for $\mu < 0.7$, the thickness of the eroded projectile element is given by,

$$\tau(\beta) = \frac{\left(1-\mu^2\right)}{2r(\beta)} . \tag{15}$$

Since the pressure force is acting normal to the flow at radius r, the centrifugal forces in the eroded element for the outside of the stagnation region must be balanced by the resistance which is equal to the pressure force plus the strength of the target,

$$R_t + \frac{1}{2}\rho_t U^2 \sin^3\beta = \tau(\beta)\,\rho_p \frac{(V-U)^2}{R(\beta)} , \tag{16}$$

where $R(\beta)$ is the scaled local radius of curvature of the center line curve. From geometric relations,

$$R(\beta) = -\frac{1}{\sin\beta}\frac{dr}{d\beta} . \tag{17}$$

Combining Eqs. (15), (16), and (17) gives the differential equation describing the trajectory of an eroded tubular element,

$$R_t + \frac{1}{2}\rho_t U^2 \sin^3\beta = -\frac{\left(1-\mu^2\right)}{2r}\rho_p(V-U)^2 \sin\beta\,(\frac{dr}{d\beta})^{-1} . \tag{18}$$

By introducing constants,

$$S = \frac{1/2\rho_p(V-U)^2}{R_t} , \qquad T = \frac{1/2\rho_t U^2}{R_t} , \tag{19}$$

7

Eq. (18) becomes,

$$2r\,dr = -\frac{2(1-\mu^2)\,S\,\sin\beta}{1+T\,\sin^3\beta}\,d\beta .$$ (20)

To determine the trajectory of an eroded element as a function of β, this equation is to be integrated with an initial condition $r\,(\beta = \pi/2) = r_1$, which yields,

$$r\,(\beta) = \sqrt{r_1^2 - \int_{90}^{\beta}\frac{2(1-\mu^2)\,S\,\sin\beta}{1+T\,\sin^3\beta}\,d\beta} .$$ (21)

By integrating Eq. (21) numerically for the domain of $0 \le \beta \le \pi/2$, the cavity radius due to the first stage (a_{c1}), can be determined. Following Miller's hypothesis that there is a stagnation region in which the pressure is equal to $1/2\rho_t U^2$, the initial condition should be estimated. It is useful to recognize that if the target pressure is approximated to be $1/2\rho_t U^2 \sin^2\beta$, there is a simple closed-form solution given by,

$$r(\beta = 0°) = a_{c1} = \sqrt{r_1^2 + \frac{(1-\mu^2)\,S}{\sqrt{T+T^2}}\,ln\left[\,1 + 2T + 2\sqrt{T+T^2}\,\right]} .$$ (22)

To find the initial condition r_1, by the same reasoning as above, Eq. (16) can be written inside the stagnation region as,

$$R_t + \frac{1}{2}\rho_t U^2 = \tau(\beta)\,\rho_p\,\frac{(V-U)^2}{R(\beta)} .$$ (23)

Again by using the radius of curvature and the thickness of the eroded element, this equation is integrated with an initial condition $r\,(\beta = \pi) = (1+\mu)/2$, which yields,

$$r_1 = \sqrt{\frac{(1+\mu)^2}{4} + \frac{2(1-\mu^2)S}{1+T}} .$$ (24)

2. The Second Stage Cavity Expansion

In addition to the first cavity expansion due to the centrifugal forces exerted by the eroded penetrator elements, the inertia imparted to the target is responsible for further cavity expansion. This inertia is created by flow in the target around a penetrator head moving at constant velocity U. In order to estimate the additional cavity expansion due to target inertia, we consider the target response to an "equivalent penetrator" — a rigid body of the same shape penetrator head

8

and penetration velocity. We can then use the energy method described previously.

Consider a rigid penetrator moving through the target with Poncelet resistance. The force (energy per unit target length) may then be written as follows,

$$F = A + BU^2 ,$$ (25)

where,

$$A = \pi\left(a_{c1}^2 - \mu^2\right)R_t, \qquad B = 1/2\pi\left(a_{c1}^2 - \mu^2\right)C_d\rho_t .$$ (26)

Here C_d is the drag coefficient. In these equations, A is the target resistance force associated with plastic work and B is the drag force which comes about due to the convective inertia effects. For the second stage this inertia is responsible for the cavity expansion from a_{c1} to a_c. Hence,

$$\frac{1}{2}\pi\left(a_{c1}^2 - \mu^2\right)C_d\rho_t U^2 = \int_{a_{c1}}^{a_c} 2\pi r R_t dr = \pi\left(a_c^2 - a_{c1}^2\right) R_t .$$ (27)

The solution for the final crater size is then given by,

$$a_c = a_{c1}\sqrt{1 + \frac{1/4\left(1-(\mu/a_{c1})^2\right)\rho_t U^2}{R_t}} .$$ (28)

The drag coefficient is assumed to be 0.5. The extent of the compensation due to inertia increases with impact velocity because the U^2 term in Eq. (28) becomes more important in the high impact velocity limit.

V. NUMERICAL SIMULATIONS

Numerical simulations of tungsten long tubular penetrators ($L/D_{eff} = 10$) into infinite RHA steel targets were conducted using an AUTODYN-2D finite difference code. The objective of the simulations was to confirm the phenomenological assumptions made in the analytical models, and to compare numerical results to the analytical predictions.

We use thick walled tubes of equivalent mass and length (78mm). The mass effective diameter of a tube is defined as

$$D_{eff} = D_o\sqrt{1 - \left(\frac{D_i}{D_o}\right)^2} ,$$ (29)

9

where D_i, D_o denote the inner and outer diameters. The dimensions of the tubular penetrators simulated are summarized in Table I. Thus the outer radius $(D_o/2)$ varies with μ.

Table I. Summary of Penetrator Dimensions

$\mu\,(D_i/D_o)$	0	0.4	0.5	0.6	0.74
D_i (mm)	0	4.25	4.50	5.85	8.58
D_o (mm)	7.8	8.51	9.01	9.75	11.60

We use a constant shear modulus G and a von-Mises yield surface with a yield strength Y as shown in Table II.

Table II. Shear Stress Parameters

	Steel	Tungsten Alloy
G (GPa)	120	140
Y (GPa)	1.2	2

AUTODYN is an Eulerian wave propagation code allowing for a maximum grid of 60,000 cells. The Mie-Gruniesen equation of state (E.O.S.) is used for both materials. The parameters are the same as in Ref. [7] and listed in Table III.

In all runs, a constant subgrid with 5-8 cells across the tubular wall and continuing for two diameters away from the tubular wall is used. Thus the cell size varies with μ. The penetration direction has a constant cell size to make the subgrid a 1:1 aspect ratio.

Table III. E.O.S Parameters

	Steel	Tungsten Alloy
ρ_o (g/cc)	7.86	17.4
c (km/s)	3.57	4.03
s	1.92	1.26
Γ_o	1.7	1.7
P_{min} (GPa)	-2	-2

The shape of the crater from 2.6 km/s impact of thin ($\mu = 0.74$) and thick ($\mu = 0.6$) tubular cases as shown in Fig. 3 exhibits the onset condition given by Franzen [2]. For $\mu = 0.74$, some fraction of the penetrator material flows inside the tube. For

10

μ = 0.6, a high stagnation pressure formed near the axisymmetric center pushes most of the penetrator material to the outside cavity. However, some target material flows to the inside cavity.

TUBE(0.6) INTO RHA(2.6KM/S)

(a)

TUBE(0.74) INTO RHA(2.6KM/S)
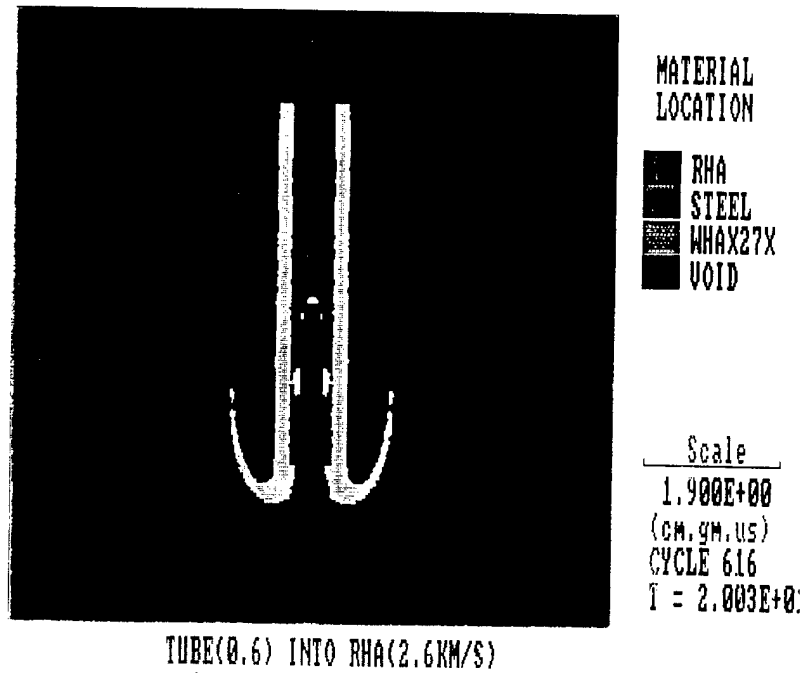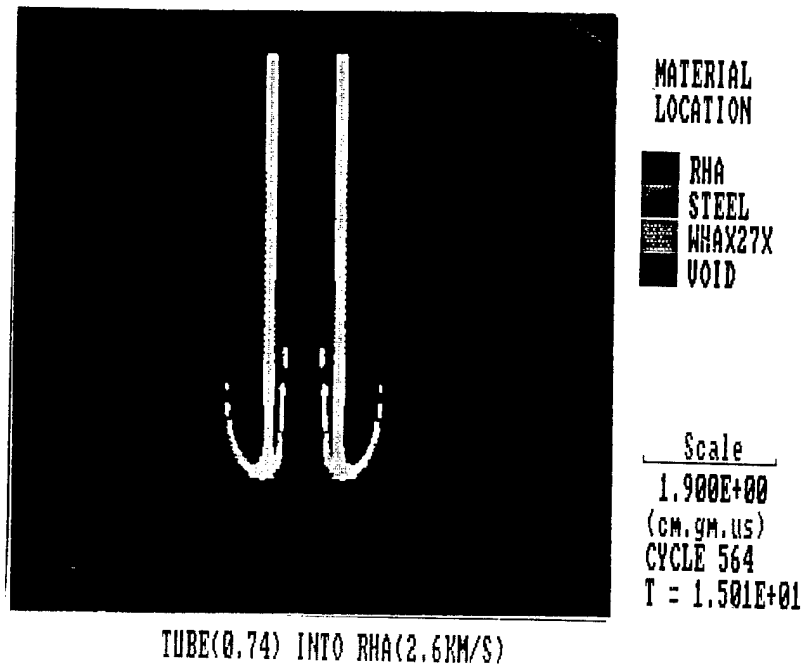
(b)

Fig. 3. Crater and penetrator configuration for (a) μ=0.6, (b) μ=0.74.

11

In Fig. 4, we show the penetration-length (PL) curves obtained from numerical simulations for tubular penetrators impacting at 2.6 km/s. The slope increases with increasing μ, approaching the rod case. For $\mu < 0.74$, the slope is almost the same during the first half of the penetration.
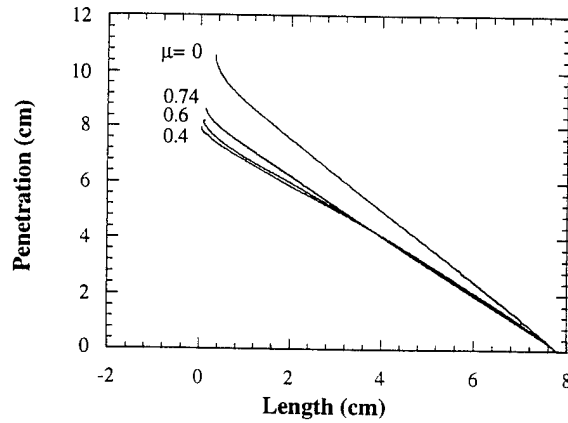

Fig. 4. Penetration-length curves. Tungsten alloy striking RHA at 2.6 km/s.

Figure 5 shows the penetration depth normalized by the penetrator length obtained from the numerical simulations for tubular penetrators impacting at 2.6 km/s and 2.2 km/s. The horizontal axis represents the diameter ratio of the tubular penetrator. This data set for thick tubular penetrators can best be represented by taking $\lambda = 3/4$, independent of μ and impact velocity. Using Eq. (10), the penetration velocity of a tubular penetrator is thus expressed by,

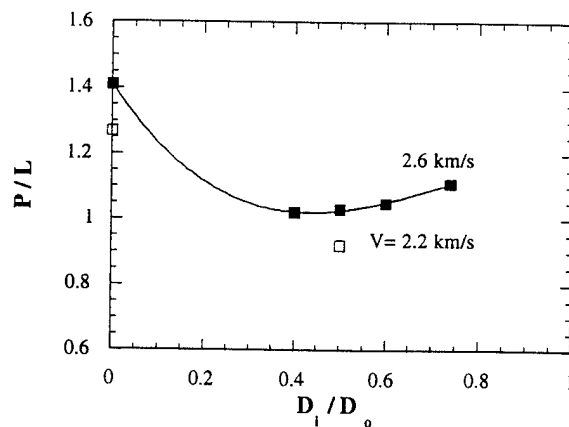$$U_{tp} = \frac{3VU_{rp}}{4V - U_{rp}} \qquad (30)$$

Fig. 5. Penetration efficiency as function of the diameter ratio, tungsten alloy striking RHA at 2.6 km/s.

VI. PREDICTIONS FOR STEEL TUBES

Penetration of steel tubes is a subject of considerable interest currently at IAT. Therefore, we apply the TSCEM to the problem of steel tubes striking RHA in order to provide some design guidance.

The case of most interest is for $\mu = 2/3$. Numerical simulations of RHA tubular penetrators $(L/D_{eff} = 10)$ into infinite RHA steel targets were conducted using AUTODYN-2D for $\mu = 0$, $\mu = 0.4$ and $\mu = 2/3$ in order to evaluate λ at 2.6 km/s. In Fig. 6, we show the penetration-length (PL) curves obtained from numerical simulations for steel tubular penetrators impacting at 2.6 km/s.
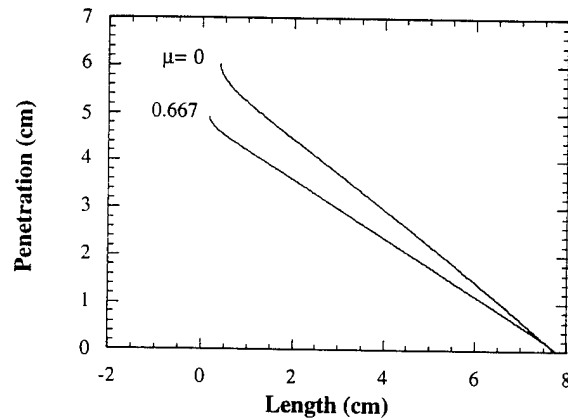

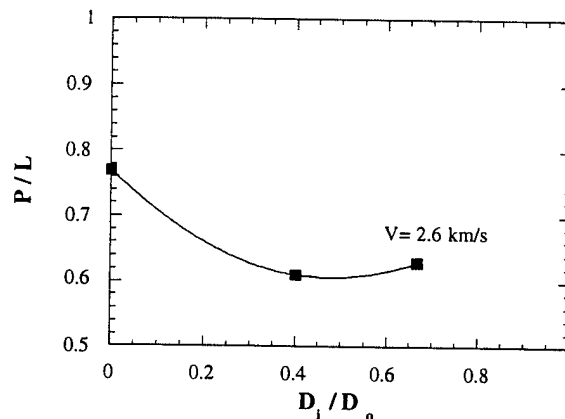**Fig. 6. Penetration-length curves, RHA striking RHA at 2.6 km/s.**

Fig. 7. Penetration efficiency, RHA striking RHA at 2.6 km/s.

Figure 7 shows the penetration depth normalized by the penetrator length obtained from the numerical simulations for steel tubular penetrators. This data set for thick tubular penetrators can best be represented by taking $\lambda = 0.8$ independent of μ.

13

VII. COMPARISON OF ANALYTICAL AND NUMERICAL RESULTS

The cavity diameters normalized by the penetrator diameters obtained from the analytical models versus impact velocity are shown in Fig. 8 for $\mu = 0.5$ case. The numerical results obtained by using AUTODYN-2D are also compared with the analytical predictions. The numerical results always underestimate the crater size, as also shown in the work of Lee and Bless [3].

As shown in Fig. 8, the results obtained from TSCEM compare well with the other analyses. It should be emphasized that the model based on energy conservation provides an upper bound for the final crater size because energy losses due to penetrator deformation, heat and strain energy in the target are ignored. However, the results from the momentum principle are almost the same as those from the energy argument, or even slightly larger. The possible explanation for this is that too large a static pressure, the second term in Eq. (14), is assumed to be generated near the axisymmetric center location.
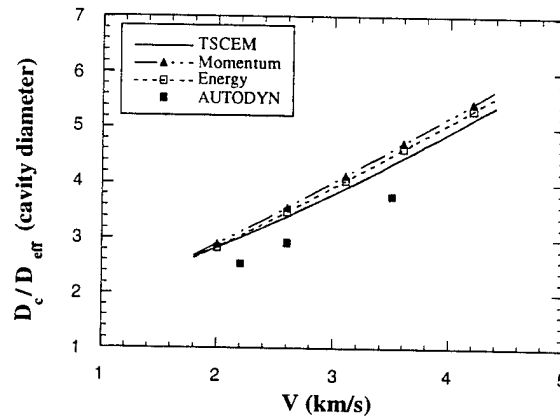
Fig. 8. Ratio of cavity diameter to tubular effective diameter vs. impact velocity. Tungsten alloy of $\mu = 0.5$ striking RHA steel target. TSCEM represents results from the two stage cavity expansion. Momentum represents results from the momentum principle and energy from the energy principle. AUTODYN represents results obtained with the AUTODYN wavecode.

In Fig. 9, the cavity diameter normalized by the penetrator diameter versus ratio of the inner to outer diameter are displayed for tungsten alloy penetrators striking RHA at 2.6 km/s. We see that the crater diameter increases slightly with increasing diameter ratio. In the calculations, the same penetration velocity is used for $\mu < 0.6$ tubes.
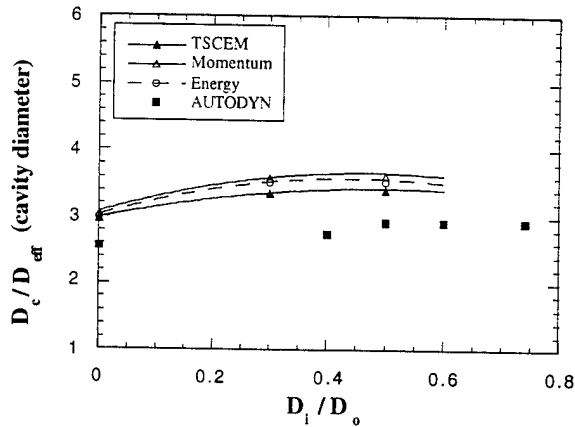
Fig. 9. Ratio of cavity diameter to tubular effective diameter as a function of diameter ratio. Tungsten alloy striking RHA steel target at 2.6 km/s.

In Fig. 10, the cavity diameter normalized by the penetrator diameter versus ratio of the inner to outer diameter are displayed for a RHA penetrator striking into a RHA target at 2.6 km/s. In the numerical simulations, the penetration efficiency (P/L) of thick and thin RHA tubes is found to be 80% of that of rod penetrators.
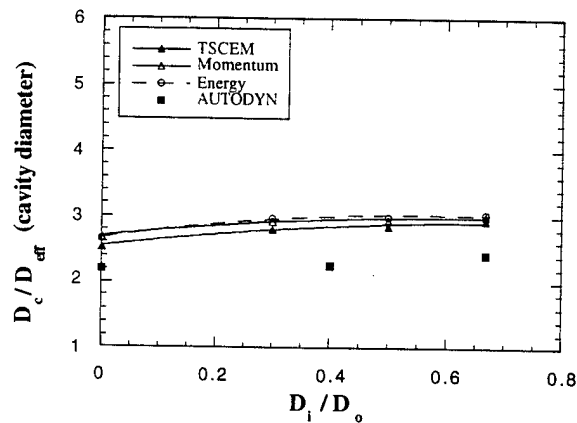

Fig. 10. Ratio of cavity diameter to tubular effective diameter as a function of diameter ratio. RHA striking RHA steel target at 2.6 km/s.

VIII. CONCLUSIONS

The penetration mechanics of long tubular penetrators are examined analytically and numerically as the ratio of the outer to inner diameter is increased from values of 0.4 to 0.74, with special interest in the thick tubes.

Analytical models for describing the final crater size are presented in three ways with many simplifications, which might impose limits on the validity of the analyses.

15

The penetration efficiency (P/L) of thick ($0.4<\mu<0.6$) and thin ($\mu = 0.74$) tungsten tubes is found to be 75% and 80% of that of rod penetrators, respectively. For example, if $U = 0.5V$ and in the hydrodynamic limit, the corresponding steady state penetration velocity for thick tubes is 86%, and for thin tubes ($\mu = 0.74$) is 89%, of the rod value. Steel tubes are slightly more efficient (relative to steel rods) than tungsten tubes.

The dependence of crater radius on velocity is almost linear, but has a slight position curvature. This is similar to the result for solid rods [3]. For both tungsten and steel tubes, of constant cross-sectional areas, as the ID/OD ratio is increased the cavity diameter increases to a maximum at about 0.5, but the increase is less than 10%. Thus, there is little flexibility in controlling crater diameter by varying ID/OD ratios.

ACKNOWLEDGMENTS

REFERENCES

[1]   Y. Kivity and E. Hirsch, "Penetration Cutoff Velocity for Ideal Jets," Ballistics' 87, 10th Int. Symp., San Diego, Ca., 1987.

[2]   Roland R. Franzen, "Notes on Tubular Hypervelocity Penetrators," Ballistics' 87, 10th Int. Symp., San Diego, CA., 1987.

[3]   M. Lee and S. Bless, "Cavity Dynamics for Long Rod Penetration," IAT.R 0094, January 1996.

[4]   A. Tate, "Long Rod Penetration Models - Part II. Extensions to the Hydrodynamic Theory of Penetration," *Int. J. Mech. Sci.*, vol. 28, no. 9, pp. 599-612, 1986.

[5]   S. Satapathy and S. Bless, "Quasi-Static Penetration Tests of PMMA: Analysis of Strength and Crack Morphology," submitted for publication to *J. Mech. Mat'ls.*, 1995.

[6]   C. W. Miller, "Two-Dimensional Engineering Model of Jet Penetration," Ballistics' 95, 15th Int. Symp., Israel, 1995.

[7]   Y. Partom, "Projectile-Flow Effect for Long Rod Penetration," Ballistics' 95 15th Int. Symp., Israel, 1995.

Distribution List

Administrator
Defense Technical Information Center
Attn: DTIC-DDA
8725 John J. Kingman Road, Ste 0944
Ft. Belvoir, VA 22060-6218

Dr. Stephan Bless
Institute for Advanced Technology
The University of Texas at Austin
4030-2 W. Braker Lane, Suite 200
Austin, TX   78759

Thomas L. Menna
General Research Corporation
5383 Hollister Ave.
Santa Barbara, CA 93111

Director
US Army Research Lab
ATTN: AMSRL OP SD TA
2800 Powder Mill Road
Adelphi, MD 20783-1145

W. deRosset
U.S. Army Research Laboratory
Attn: AMSRL-WT-TC
Aberdeen Prvg Grd, MD 21005-5066

Mr. Dennis L. Orphal
The Titan Corporation
California Research & Technology Division
5117 Johnson Drive
Pleasanton, CA 94566

Director
US Army Research Lab
ATTN: AMSRL OP SD TL
2800 Powder Mill Road
Adelphi, MD 20783-1145

Dr. Joe Foster
Air Force Armament & Technology Lab
AFATL/MNW
Eglin AFB, FL 32542

A. M. Rajendran
US Army Research Lab
Arsenal St.
Watertown, MA 02172

Director
US Army Research Lab
ATTN: AMSRL OP SD TP
2800 Powder Mill Road
Adelphi, MD   20783-1145

K. Frank
U.S. Army Research Laboratory
Attn: AMSRL-WT-TD
Aberdeen Prvg Grd, MD 21005-5066

Edward Schmidt
U.S. Army Research Laboratory
Attn: AMSRL-WT-PB
Aberdeen Prvg Grd, MD 21005-5066

Army Research Laboratory
AMSRL-CI-LP
Technical Library 305
Aberdeen Prvg Grd, MD 21005-5066

W. J. Gillich
U.S. Army Research Laboratory
AMSRL-WT-TA
Aberdeen Prvg Grd, MD 21005-5066

Dr. Charles Anderson, Jr.
Southwest Research Institute
Engineering Dynamics Department
P.O. Box 28510
San Antonio, TX 78228-0510

Tim Holmquist
Alliant Techsystems, Inc.
Twin City Army Ammunition Plant-Bldg. 103
New Brighton, MN 55112

T. Bjerke
Director
U.S. Army Research Laboratory
Attn: AMSRL-WT-TC
Aberdeen Prvg Grd, MD 21005-5066

Nick Lynch
DERA Fort Halstead
Bldg. A 20, Div. WX5
Sevenoaks, Kent
England TN14 7BP